

# Near-infrared integrated spectra of Galactic globular clusters: testing simple stellar population models

R. Riffel<sup>1\*</sup>, D. Ruschel-Dutra<sup>1</sup>, M. G. Pastoriza<sup>1</sup>, A. Rodríguez-Ardila<sup>2</sup>,  
J. F. C. Santos Jr.<sup>3</sup>, C. J. Bonatto<sup>1</sup> and J. R. Ducati<sup>1</sup>

<sup>1</sup>*Departamento de Astronomia, Universidade Federal do Rio Grande do Sul. Av. Bento Gonçalves 9500, Porto Alegre, RS, Brazil.*

<sup>2</sup>*Laboratório Nacional de Astrofísica/MCT - Rua dos Estados Unidos 154, Bairro das Nações - Itajubá - MG, Brazil.*

<sup>3</sup>*Dep. de Física -ICEX - UFMG, Campus da Pampulha, Av. Antonio Carlos 6627, 31270-901 - Belo Horizonte - MG, Brazil.*

## ABSTRACT

We present SOAR/OSIRIS cross-dispersed near-infrared (NIR) integrated spectra of 12 Galactic globular clusters that are employed to test Maraston (2005, hereafter M05) NIR Evolutionary Population Synthesis (EPS) models, and to provide spectral observational constraints to calibrate future models. We measured Equivalent Widths ( $W_\lambda$ ) of the most prominent NIR absorption features:  $\lambda$  1.49  $\mu\text{m}$ , Mg I  $\lambda$  1.58  $\mu\text{m}$ , Fe I/Mg I,  $\lambda$  1.59  $\mu\text{m}$ , Si I,  $\lambda$  1.71  $\mu\text{m}$ , Mg I,  $\lambda$  2.21  $\mu\text{m}$ , Na I and  $\lambda$  2.26  $\mu\text{m}$ , Ca I as well as the  $\lambda$  1.62  $\mu\text{m}$ ,  $\lambda$  2.29  $\mu\text{m}$ , CO and  $\lambda$  2.05  $\mu\text{m}$ , CN molecular bands. Optical  $W_\lambda$  of G-band (4300 Å), H $\beta$ , Mg<sub>2</sub>, Fe I (4531 Å, 527 Å and 5335 Å), and Na I (5897 Å) were also measured. The globular clusters  $W_\lambda$  were compared with model predictions with ages within 4 — 15 Gyr, and metallicities between  $\frac{1}{200} Z_\odot$  and  $2 Z_\odot$ . Observed integrated colours ( $B - V$ ,  $V - I$  and  $V - K_s$ ) were also compared with models. The NIR integrated spectra among our sample appear qualitatively similar in most the absorption features. The M05 models can properly predict the optical  $W_\lambda$  observed in globular clusters. Regarding the NIR, they do underestimate the strength of Mg I 1.49  $\mu\text{m}$ , but they can reproduce the observed  $W_\lambda$  of Fe I 1.58  $\mu\text{m}$ , Si I 1.59  $\mu\text{m}$ , and CO 2.29  $\mu\text{m}$ , in about half of our sample. The remaining objects require the inclusion of intermediate-age populations. Thus, we suggest that the presence of C- and O-rich stars in models is important to reproduce the observed strengths of metallic lines. Another possibility is the lack of  $\alpha$ -enhancement in the models. In the case of the optical and NIR Fe I lines, standard models and those that include blue horizontal branch stars, produce similar results. A similar trend is observed for Na I 5895 Å, while in the case of the G-band, the models with blue horizontal branch do describe better the observations. For most of the sample the optical to NIR colours are well described by the M05 models. In general, M05 models can provide reliable information on the NIR stellar population of galaxies, but only when  $W_\lambda$  and colours are taken together, in other words,  $W_\lambda$  and continuum fluxes should be simultaneously fitted. However, the results should be taken with caution, since the models tend to predict results biased towards young ages.

**Key words:** Globular clusters: general, Galaxy: stellar content, Near Infrared

## 1 INTRODUCTION

The study of stellar populations is a critical step to understand the continuum emission of galaxies, even in active galactic nuclei (AGN). This occurs because several components such as the non-thermal continuum, dust emission, the presence of an active nucleus, and the stellar population itself, sum up to the integrated spectrum. By analysing the stellar content, information can be obtained on critical processes like recent star formation episodes, the evolutionary history of the galaxy, and the connection between the active galactic nucleus and starburst activity.

Observations in the near-infrared (NIR) are important to study the integrated stellar populations of galaxies, since this is the most convenient spectral region accessible to ground-based telescopes to probe highly obscured sources. However, tracking the star formation in the NIR is complicated (Origlia & Oliva 2000). Nevertheless, NIR stellar absorption features are widely believed to provide means for recognising red supergiants (Oliva et al. 1995), since they arise as prime indicators for tracing starbursts in galaxies. Besides the short-lived red supergiants, the NIR also includes the contribution of thermally-pulsating asymptotic giant branch (TP-AGB) stars, enhanced in young to intermediate age stellar populations ( $0.2 \leq t \leq 2$  Gyr, Maraston 1998, 2005; Riffel et al. 2007, 2008, 2009). The TP-AGB phase becomes fully developed in stars

\* E-mail: riffel@ufrgs.br

with a degenerate carbon oxygen core (see Iben & Renzini 1983, for a review). Evidence of this population in the optical is usually missed, as the most prominent spectral features associated with this evolutionary phase falls in the NIR (Maraston 2005, hereafter M05).

Usually, the interpretation of a galaxy's stellar population involves a synthesis approach that, in general, is based on the mixing of simple stellar populations of different ages and metallicities that provides the best match to the galaxy spectra. The combinations can be done using equivalent widths ( $W_\lambda$ ) and selected continuum fluxes (e.g. Bica & Alloin 1986; Bica 1988; Riffel et al. 2008) or by fitting the whole underlying spectrum (e.g. Cid Fernandes et al. 2004, 2005a,b; Asari et al. 2007; Cid Fernandes et al. 2008; Riffel et al. 2009). However, in both methods the most important ingredient in the SP synthesis is the spectral base. An ideal base should cover the full range of spectral properties that occurs in a galaxy sample, providing enough resolution in age and metallicity to properly address the desired scientific question (see Schmidt et al. 1991; Cid Fernandes et al. 2005a, for example).

A reliable base to probe the stellar population of galaxies is a library of integrated spectra of star clusters such as the one constructed by Bica & Alloin (1986). However this base is restricted to the optical region and metallicities lower than solar ( $[Z/Z_\odot] \lesssim 0.1$ ). The main advantage of this approach over those based on spectra of individual stars, the so called Evolutionary Population Synthesis (EPS) models (Bruzual & Charlot 2003; Vazdekis et al. 2010, M05), is the reduced number of variables. While the latter are essentially described by the temperature, gravity and metallicity, uncertainties in the former are reduced to age and metallicity. Also, Bica & Alloin (1986) method is free from any assumptions on stellar evolution and the initial mass function. However, one advantage of the EPS models is their large range in ages and metallicities, while observed spectral libraries are restricted to the optical (e.g. Bica & Alloin 1986) or cover only small fractions of the NIR spectral region, like the region around the  $1.6\mu\text{m}$  and  $2.29\mu\text{m}$  CO bands (Origlia et al. 1994, 1997) or only the  $K$ -band spectra (Lyubenova 2010).

The above considerations justify a project to check the reliability of NIR EPS models available in the literature and to set important constraints on the absorption features observed in this spectral region. We focus here on the observation of NIR ( $\sim 1.2\mu\text{m}$ – $2.35\mu\text{m}$ ) integrated spectra of globular clusters. By their very nature, globular clusters spectra should be reproduced by simple stellar population theoretical models.

This paper is structured as follows: In section 2 observations and data reduction procedures are described. Results are presented and discussed in section 3, and conclusions are presented in section 4.

## 2 SAMPLE SELECTION, OBSERVATIONS AND DATA REDUCTION

As part of an ongoing project to investigate NIR spectral properties of globular clusters, we have selected a representative sub-sample of the star clusters from Bica & Alloin (1986) to test NIR EPS models. Our original sample was composed by 27 star clusters covering almost all the possibilities of the age/metallicity that occur in galaxies.

As stated by M05, even bright optical star clusters have the NIR light dominated by stars in short-lived evolutionary phases like

**Table 1.** Observation log.

| Object<br>(NGC) | Exp. Time<br>(s) | S/N | Date       | Object<br>(NGC) | Exp. Time<br>(s) | S/N | Date       |
|-----------------|------------------|-----|------------|-----------------|------------------|-----|------------|
| 104             | 144              | 55  | 10/01/2006 | 6517            | 3120             | 65  | 06/10/2009 |
| 362             | 170              | 45  | 10/01/2006 | 6528            | 1680             | 52  | 06/09/2009 |
| 1851            | 360              | 54  | 10/24/2006 | 6541            | 1920             | 43  | 06/10/2009 |
| 2808            | 255              | 35  | 12/17/2006 | 6553            | 600              | 63  | 06/09/2009 |
| 6388            | 480              | 30  | 06/09/2009 | 6864            | 72               | 30  | 10/24/2006 |
| 6440            | 840              | 27  | 06/09/2009 | 7078            | 340              | 46  | 10/24/2006 |

S/N measured in the  $K$ -band spectra.

the bright red giant branch (RGB), as well as the TP-AGB. Thus, to avoid the resolution of individual stars, two strategies were used: (i) the telescope was defocused and (ii) non sidereal guiding, sweeping the area corresponding to the cluster centre. Consequently, integrated spectra of the mixed light of a representative fraction of the cluster stars were obtained.

Using these strategies, cross-dispersed (XD) NIR spectra of 23 star clusters were obtained from October 2006 to June 2009, at the Ohio State Infrared Imager/Spectrometer (OSIRIS) attached to the 4.1 m Southern Astrophysical Research (SOAR) Telescope. The detector is a  $1024 \times 1024$  HgCdTe array. At the XD mode the spectrograph provides simultaneous coverage of the region between  $1.2\mu\text{m}$  and  $2.35\mu\text{m}$  with a resolving power of  $R \sim 1200$ . It is interesting to note that in this mode it is possible to observe the  $1.2\mu\text{m}$  to  $2.35\mu\text{m}$  region in a single shot, avoiding the seeing and aperture effects when observing in single bands.

Because of the extended nature of the science targets, it was necessary to take separate sky exposures, following the pattern ABAB, where A is the on-source observation, with the object centred on the slit, and B represents off-source exposures. To remove telluric lines and to flux calibrate the spectra, standard stars were observed, following the nod pattern along the slit.

Given the nature of the NIR light emitted by globular clusters, the above observational strategy and configuration produced only 12 reliable ( $S/N \gtrsim 25$ ) integrated spectra of globular clusters (Tab.1). We list their observed colours and some basic properties in Tab. 2. As it can be seen from Tab. 2 and Fig. 1 of Bica et al. (2006), seven clusters are metal-poor, while the metal-rich ones are almost all located in the Galactic bulge ( $d_{GC} \leq 5\text{kpc}$ ).

The spectral reduction, extraction and wavelength calibration procedures were performed using XD-Spres<sup>1</sup> IRAF software task (Ruschel-Dutra et al. 2010, *in preparation*). This tool follows the standard NIR cross dispersed reduction procedures, as listed: (i) to remove sky emission lines from the integrated spectra, sky exposures were subtracted from the object. (ii) the resulting images were summed up and then divided by a normalised flat-field image. (iii) extraction was performed following the standard echelle procedures. (iv) wavelength calibration was based on the OH lines present in the sky exposures with the values given by Oliva & Origlia (1992). (v) the 1-D spectra were then corrected for telluric absorption by comparison with an A0V star spectrum. The stellar atmospheric absorption lines were identified and removed. This procedure was done using the TELLURIC task. (vi) finally, the flux calibration was achieved by fitting a black-body curve to the

<sup>1</sup> <http://www.if.ufrgs.br/~riffel/software.html>.

**Table 2.** Observed colours and some basic properties of the cluster sample.

| Data Unit | l (deg) | b (deg) | dGC (kpc) | [Fe/H] | Mv (mag) | (J-Ks) (mag) | (J-H) (mag) | (H-Ks) (mag) | (V-Ks) (mag) | (U-B) (mag) | (B-V) (mag) | (V-R) (mag) | (V-I) (mag) |
|-----------|---------|---------|-----------|--------|----------|--------------|-------------|--------------|--------------|-------------|-------------|-------------|-------------|
| NGC       | (a)     | (a)     | (a)       | (a)    | (b)      | (c)          | (c)         | (c)          | (c)          | (b)         | (b)         | (b)         | (b)         |
| 104       | 305.90  | -44.89  | 6.7       | -0.76  | -9.42    | 0.74±0.03    | 0.55±0.03   | 0.19±0.04    | 2.60         | 0.37        | 0.88        | 0.53        | 1.14        |
| 362       | 301.53  | -46.25  | 8.9       | -1.16  | -8.40    | 0.64±0.03    | 0.52±0.03   | 0.12±0.04    | 2.53         | 0.16        | 0.77        | 0.49        | 1.01        |
| 1851      | 244.51  | -35.04  | 16.1      | -1.22  | -8.33    | 0.65±0.03    | 0.53±0.03   | 0.12±0.04    | 2.66         | 0.17        | 0.76        | 0.49        | 1.01        |
| 2808      | 282.19  | -11.25  | 10.5      | -1.15  | -9.36    | 0.62±0.03    | 0.51±0.25   | 0.11±0.25    | 2.50         | 0.23        | 0.92        | 0.57        | 1.18        |
| 6388      | 345.56  | -6.74   | 5.0       | -0.60  | -9.82    | 0.75±0.03    | 0.62±0.03   | 0.13±0.04    | 2.65         | 0.66        | 1.17        | 0.71        | 1.47        |
| 6440      | 7.73    | +3.80   | 1.7       | -0.34  | -8.75    | 0.74±0.03    | 0.66±0.03   | 0.08±0.04    | 3.06         | 1.47        | 1.97        | 1.24        | 2.51        |
| 6517      | 19.23   | +6.76   | 4.7       | -1.37  | -8.28    | 0.49±0.03    | 0.48±0.03   | 0.01±0.04    | 3.22         | 0.85        | 1.75        | –           | 2.31        |
| 6528      | 1.14    | -4.17   | 2.0       | -0.04  | -6.93    | 0.78±0.03    | 0.65±0.03   | 0.13±0.04    | 4.04         | 1.09        | 1.53        | 0.9         | 1.74        |
| 6541      | 349.29  | -11.18  | 1.9       | -1.83  | -8.37    | 0.42±0.15    | 0.41±0.13   | 0.01±0.19    | 2.33         | 0.13        | 0.76        | 0.49        | 1.01        |
| 6553      | 5.25    | -3.02   | 1.7       | -0.21  | -7.99    | 0.87±0.03    | 0.69±0.03   | 0.18±0.04    | 3.73         | 1.34        | 1.73        | 1.01        | 2.13        |
| 6864      | 20.30   | -25.75  | 14.6      | -1.16  | -8.35    | 0.61±0.03    | 0.52±0.03   | 0.09±0.04    | 2.36         | 0.28        | 0.87        | 0.55        | 1.16        |
| 7078      | 65.01   | -27.31  | 10.1      | -1.62  | -9.17    | 0.58±0.00    | 0.47±0.00   | 0.11±0.00    | 2.16         | 0.06        | 0.68        | –           | 0.85        |

Table Notes: (a) From Bica et al. (2006); (b) From - <http://www.physics.mcmaster.ca/Globular.html> (Harris 1996); (c) From Cohen et al. (2007).

The NIR colours are reddening-corrected (Cohen et al. 2007) while the optical ones are uncorrected (Harris 1996).

standard star featureless spectrum, using the task CALIBRATE of the IRAF software. Final reduced spectra, are shown in Fig. 1.

### 3 RESULTS AND DISCUSSION

#### 3.1 General overview of the spectra

Spectra of the 12 Galactic globular clusters covering simultaneously the NIR spectral region between  $1.2\mu\text{m}$  -  $2.35\mu\text{m}$  are presented here for the first time. The full NIR spectral energy distribution (SED) of the clusters is shown in Fig. 1. The NIR SED of the clusters is rather similar among the 12 objects analysed, decreasing smoothly in flux with wavelength, and present similar absorption features. The shaded area in Fig. 1 denotes a region highly affected by telluric absorption, thus it was left out of further analysis.

In order to highlight the absorption lines, the spectra were linearised by their continuum. The result of this process is shown in Figs. 2 to 4. Clearly, the spectra of the globular cluster sample appear qualitatively similar in most of the NIR absorption features. Such similarity can be observed in Figs. 2 to 4, where many atomic absorption features like  $\lambda$  1.49 $\mu\text{m}$  Mg I,  $\lambda$  1.58 $\mu\text{m}$  Fe I/Mg I,  $\lambda$  1.59 $\mu\text{m}$  Si I,  $\lambda$  1.71 $\mu\text{m}$  Mg I,  $\lambda$  2.21 $\mu\text{m}$  Na I and  $\lambda$  2.26 $\mu\text{m}$  Ca I as well as the  $\lambda$  1.62 $\mu\text{m}$ ,  $\lambda$  2.29 $\mu\text{m}$  CO and  $\lambda$  2.05 $\mu\text{m}$  CN molecular bands are clearly detected and identified in the spectra. The centre and width of the strongest lines are identified in Figs. 2 to 4. The similarity between the spectra is not surprising, since the sample is composed only by globular clusters and thus, the integrated spectra is dominated by stars of relatively similar spectral type.

It is also clear in Figs. 2 to 4 that the spectra show many weak absorption lines. However, as the S/N (see Tab. 1) is relatively poor, no effort was made to identify such weak absorptions. In addition, the *H* and *K*-band lines presently detected are common in the brightest stars of star clusters (Origlia, Rich & Castro 2002; Origlia et al. 2006; Frogel et al. 2001; Stephens & Frogel 2004), which indicates that our data reduction is consistent.

To date the only effort in obtaining NIR integrated spectra of Galactic star clusters was from Origlia et al. (1994, 1997). These authors used the IRSPEC infrared spectrometer (Moorwood et al. 1991) attached to the European Southern Observatory (ESO) New Technology Telescope (NTT). Their instrumental setup allowed

them to obtain long-slit spectra centred at 1.59 $\mu\text{m}$  (Si I), 1.62 $\mu\text{m}$  (CO 6-3), and 2.29 $\mu\text{m}$  (CO 2-0). These absorptions are clearly detected in our spectra (Figs. 2 - 4). For a comparison between both data sets, the  $W_\lambda$  reported by Origlia et al. (1994, 1997) for the objects in common with our sample were plotted against those measured by us (Fig. 5). The Pearson correlation coefficient ( $r^2 = 0.87$ ) and a nonlinear regression were computed using the FITEXY routine from the IDL Astronomy User's Library, which takes errors in both coordinates into account. We find  $W_\lambda = -(3.66 \pm 1.65) + (1.93 \pm 0.29) W_{\lambda, \text{lit}}$ , where  $W_\lambda$  means this work and  $W_{\lambda, \text{lit}}$  the literature data. A generalised correlation coefficient (CC=0.75), defined as the square root of the fraction of total  $y$  variance explainable by the fitted function was also computed. Clearly, there is a discrepancy between our values and those of Origlia et al. (1997). Probably, the difference in  $W_\lambda$  of Si I 1.59 $\mu\text{m}$  and CO 1.62 $\mu\text{m}$  occurs because these authors use rectified spectra, instead of locally defined continuum regions. For the 2.29 $\mu\text{m}$  CO band, the differences in  $W_\lambda$  are associated with different line definitions (see Sec. 3.2). In addition, the difference may be partly due to the fact that Origlia et al. (1994, 1997) only sampled a very small fraction of the cluster core ( $6'' \times 4''$ ). Thus, the random contribution of a few bright, red giant stars in such a small field, may strongly affect features in the integrated spectra.

#### 3.2 Equivalent Widths

A straightforward approach for comparing a set of empirical spectra with models is by means of the  $W_\lambda$  of their absorption features. Such a procedure is virtually free from flux calibration issues and reddening corrections, and may provide constraints on model predictions.

When dealing with optical absorption lines, the spectral window of a feature is usually defined together with two continuum regions at the red and blue sides, which are used to trace a local continuum through a linear fit to the mean values of both continuum regions (e.g. Faber et al. 1985; Bica & Alloin 1986). Similar definitions were made for some NIR absorption features (e.g. Oliva et al. 1995; Frogel et al. 2001), however, they were based in stellar spectra, where absorption features are typically a few  $\text{km s}^{-1}$  wide. As we are dealing with velocity-dispersion sustained ( $\sigma_v \gtrsim 10 \text{ km s}^{-1}$ )

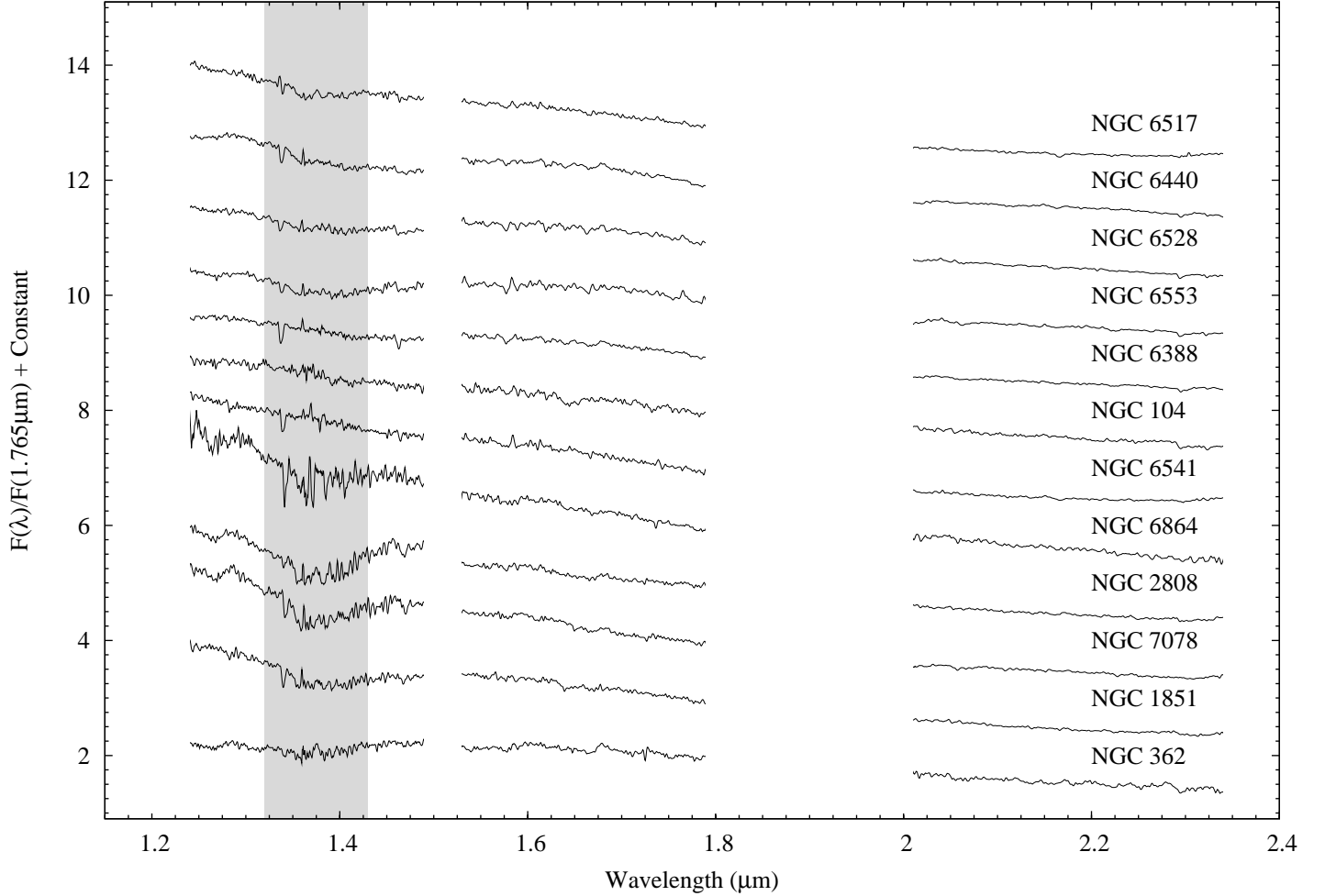


**Figure 1.** Globular Clusters NIR spectral energy distribution. The spectra were normalised by the mean value of their fluxes between  $1.76\mu\text{m}$  and  $1.77\mu\text{m}$  and shifted by a constant for display purposes. The shaded region was left out of the analysis (see text). The gaps represent regions strongly dominated by telluric absorptions, and/or coincide with band limits.

clusters, and we aim to use these absorption features to investigate unresolved stellar populations in galaxies, we are forced to use spectral indices with broader band passes than those used in individual stars. Our continuum and band-pass definitions are listed in Tab. 3. They were taken from the literature, except for Mg I  $1.49\mu\text{m}$  and CN  $2.05\mu\text{m}$ , which we define in Tab. 3. In some cases it was also necessary to re-define the continuum regions in to avoid overlap (Tab. 3). However, special care was taken to use only regions free from emission/absorption lines. An example of these continuum and line limits is shown in Fig. 6.

With the definitions for continuum and band pass listed in Tab. 3,  $W_\lambda$  was measured for nine absorption lines, using the code PACCE, which computes  $W_\lambda$  with user definitions for the line and continuum band-passes (Vale et al. 2007). The measured  $W_\lambda$  values are presented in Tab. 4. Errors were estimated according to Eq. 7 of Vollmann & Eversberg (2006).

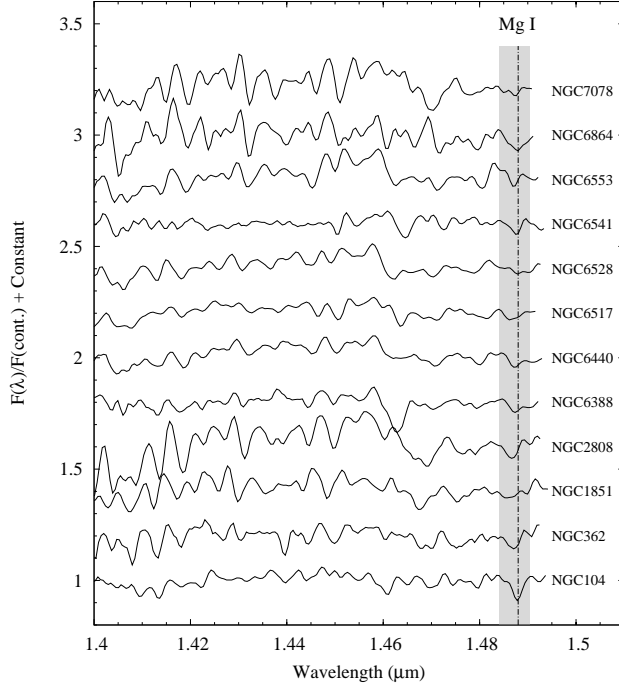
In addition, we measured on the 12 globular clusters,  $W_\lambda$  using the Lick indices definitions (e.g. Worthey et al. 1994, taken from: <http://astro.wsu.edu/worthey/html/system.html>) for the following optical features:  $G$ -band ( $4300\text{\AA}$ ), Fe I ( $4531\text{\AA}$ ,  $5270\text{\AA}$  and  $5335\text{\AA}$ ), H $\beta$ , MgH ( $5176\text{\AA}$ ), and Na I ( $5895\text{\AA}$ ), MgH ( $5176\text{\AA}$ ). The  $W_\lambda$  corresponding to the MgH absorption is called  $Mg_2$ , which is

**Table 3.** Line limits and continuum band-passes.

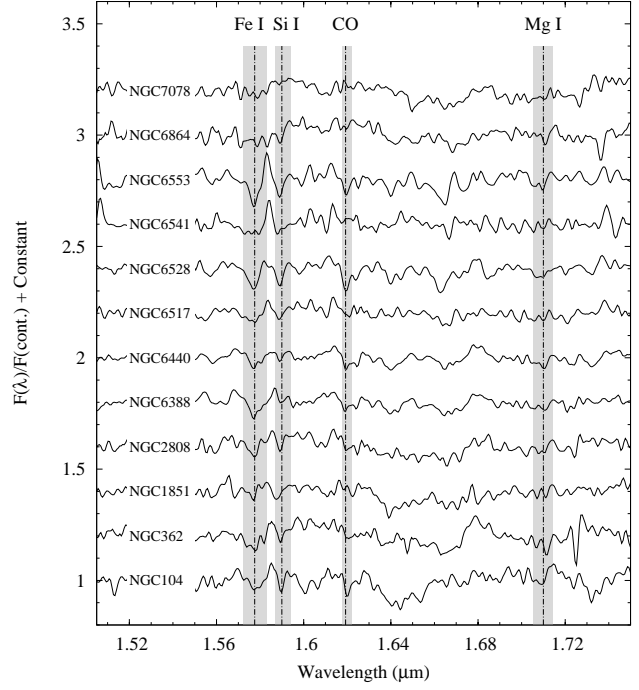
| Line                       | $EW_{\lambda b}$ | $EW_{\lambda r}$ | $CBP_b$         | $CBP_r$         |
|----------------------------|------------------|------------------|-----------------|-----------------|
| Mg I $1.49\mu\text{m}$     | 1.4840           | 1.4903           | 1.4620 - 1.4830 | 1.4910 - 1.4925 |
| Fe I $1.58\mu\text{m}$ (a) | 1.5720           | 1.5830           | 1.5400 - 1.5700 | 1.5950 - 1.6160 |
| Si I $1.59\mu\text{m}$ (b) | 1.5870           | 1.5910           | 1.5400 - 1.5700 | 1.5950 - 1.6160 |
| CO $1.62\mu\text{m}$ (b)   | 1.6175           | 1.6220           | 1.5950 - 1.6160 | 1.6280 - 1.6570 |
| Mg I $1.71\mu\text{m}$ (c) | 1.7053           | 1.7143           | 1.7010 - 1.7056 | 1.7156 - 1.7256 |
| CN $2.05\mu\text{m}$       | 2.0507           | 2.0615           | 2.0250 - 2.0350 | 2.0700 - 2.1730 |
| Na I $2.21\mu\text{m}$ (c) | 2.2000           | 2.2140           | 2.1934 - 2.1996 | 2.2150 - 2.2190 |
| Ca I $2.26\mu\text{m}$ (c) | 2.2594           | 2.2700           | 2.2516 - 2.2590 | 2.2716 - 2.2888 |
| CO $2.29\mu\text{m}$ (c)   | 2.2910           | 2.3070           | 2.2716 - 2.2888 | 2.3120 - 2.3140 |

Table Notes: Table Notes:  $CBP_b$  and  $CBP_r$  are the blue and red band-pass boundaries for the continuum. (a) from Riffel et al. (2008), (b) from Origlia et al. (1993), (c) from Cesetti et al. (2009).

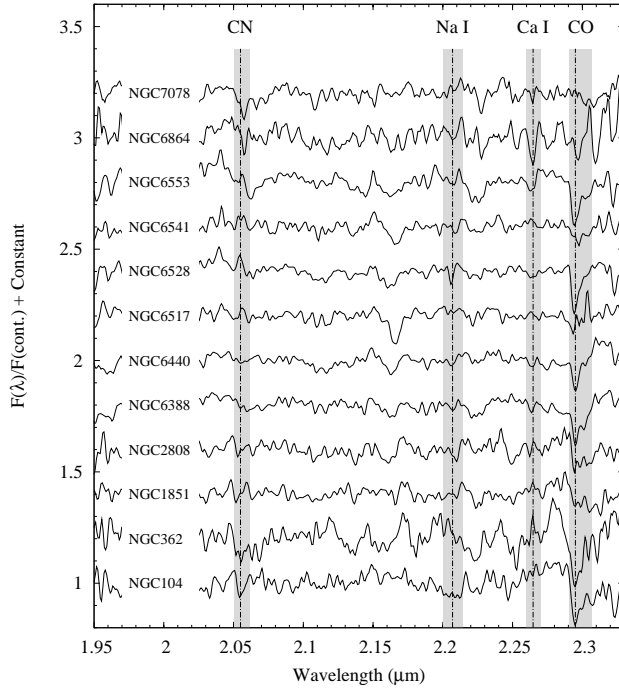
adopted in the present paper. The optical integrated spectra of the clusters were taken from Santos et al. (2002). Observation and reduction procedures, as well as data quality of the optical spectra, are discussed in Bica & Alloin (1986). The optical  $W_\lambda$  are listed in Tab. 4. Errors were estimated similarly to the NIR  $W_\lambda$ .



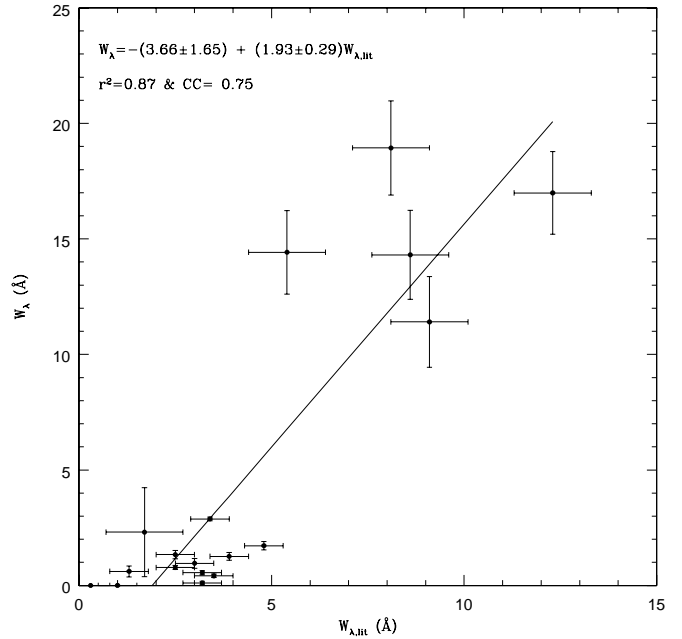
**Figure 2.** J-band final reduced spectra. The most prominent lines are identified. The shaded region represents the line limits and the vertical line shows the line centre.



**Figure 3.** H-band final reduced spectra. The most prominent lines are identified. The shaded region represents the line limits and the vertical line shows the line centre.



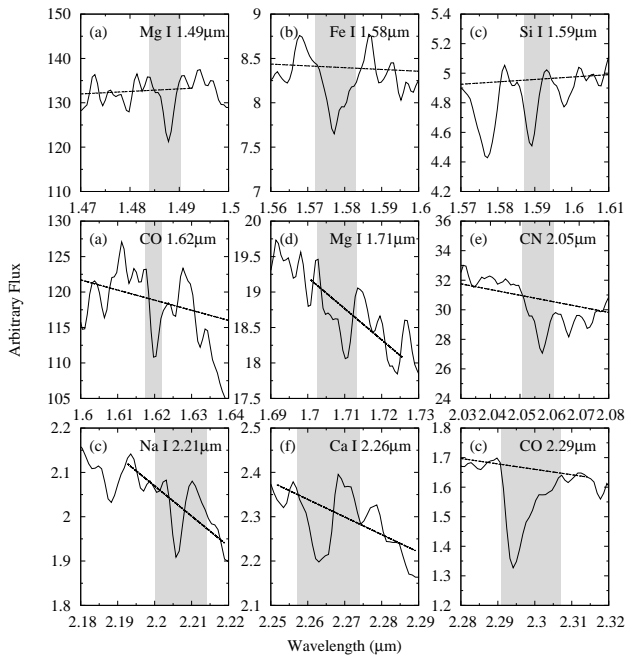
**Figure 4.** K-band final reduced spectra. The most prominent lines are identified. The shaded region represents the line limits and the vertical line shows the line centre.



**Figure 5.** Comparison of the measured  $W_\lambda$  with literature data from Origlia et al. (1997). Features used are  $1.59\mu\text{m}$  (Si I),  $1.62\mu\text{m}$  (CO 6-3),  $2.29\mu\text{m}$  (CO 2-0). The Pearson coefficient ( $r^2$ ), a generalised correlation coefficient (CC, see text) as well as the regression equation are shown.

**Table 4.** Measured  $W_\lambda$  (in Å) for the cluster sample.

| $W_\lambda$<br>NGC | G<br>4300Å      | Fe I<br>4531Å   | H $\beta$<br>4863 | Mg <sub>2</sub><br>5176Å | Fe I<br>5270    | Fe I<br>5335    | Na I<br>5895Å   | Mg I<br>1.49 $\mu$ m | Fe I<br>1.58 $\mu$ m | Si I<br>1.59 $\mu$ m | CO<br>1.62 $\mu$ m | Mg I<br>1.71 $\mu$ m | CN<br>2.05 $\mu$ m | Na I<br>2.21 $\mu$ m | Ca I<br>2.26 $\mu$ m | CO<br>2.29 $\mu$ m |
|--------------------|-----------------|-----------------|-------------------|--------------------------|-----------------|-----------------|-----------------|----------------------|----------------------|----------------------|--------------------|----------------------|--------------------|----------------------|----------------------|--------------------|
| 104                | 3.50 $\pm$ 0.24 | 1.53 $\pm$ 0.36 | 1.33 $\pm$ 0.18   | 5.26 $\pm$ 0.04          | 1.09 $\pm$ 0.16 | 1.13 $\pm$ 0.50 | 1.73 $\pm$ 0.16 | 1.59 $\pm$ 0.31      | 1.41 $\pm$ 0.25      | 0.56 $\pm$ 0.09      | 1.34 $\pm$ 0.18    | 0.58 $\pm$ 1.05      | —                  | 7.05 $\pm$ 3.48      | —                    | 18.94 $\pm$ 2.04   |
| 362                | 2.68 $\pm$ 0.23 | 1.34 $\pm$ 0.36 | 1.56 $\pm$ 0.18   | 1.33 $\pm$ 0.04          | 0.72 $\pm$ 0.16 | 0.83 $\pm$ 0.51 | 0.63 $\pm$ 0.16 | 1.05 $\pm$ 0.32      | 5.98 $\pm$ 0.24      | 1.38 $\pm$ 0.09      | 0.74 $\pm$ 0.22    | 1.97 $\pm$ 1.22      | 7.10 $\pm$ 0.16    | —                    | —                    | 23.32 $\pm$ 1.89   |
| 1851               | 1.50 $\pm$ 0.23 | 0.85 $\pm$ 0.37 | 1.57 $\pm$ 0.18   | 1.38 $\pm$ 0.04          | 1.09 $\pm$ 0.16 | 0.52 $\pm$ 0.51 | 0.62 $\pm$ 0.16 | 1.73 $\pm$ 0.31      | 0.64 $\pm$ 0.24      | 1.08 $\pm$ 0.08      | —                  | —                    | —                  | 0.52 $\pm$ 4.61      | —                    | 4.46 $\pm$ 2.07    |
| 2808               | 2.46 $\pm$ 0.23 | 2.00 $\pm$ 0.36 | 1.83 $\pm$ 0.18   | 0.96 $\pm$ 0.04          | 0.98 $\pm$ 0.16 | 0.60 $\pm$ 0.51 | 1.47 $\pm$ 0.16 | 1.15 $\pm$ 0.34      | 2.30 $\pm$ 0.24      | 0.78 $\pm$ 0.09      | 0.61 $\pm$ 0.24    | —                    | 0.25 $\pm$ 0.15    | 4.18 $\pm$ 4.19      | 0.10 $\pm$ 0.93      | 14.42 $\pm$ 1.81   |
| 6388               | 2.70 $\pm$ 0.23 | 2.14 $\pm$ 0.36 | 1.31 $\pm$ 0.18   | 4.91 $\pm$ 0.04          | 1.23 $\pm$ 0.17 | 1.18 $\pm$ 0.50 | 3.43 $\pm$ 0.15 | 1.79 $\pm$ 0.31      | 4.69 $\pm$ 0.23      | >0.11                | 0.96 $\pm$ 0.21    | 0.62 $\pm$ 1.05      | 2.93 $\pm$ 0.15    | —                    | 0.60 $\pm$ 0.96      | 14.31 $\pm$ 1.93   |
| 6440               | 3.11 $\pm$ 0.25 | 2.24 $\pm$ 0.36 | 1.81 $\pm$ 0.17   | 6.86 $\pm$ 0.07          | 0.90 $\pm$ 0.17 | 0.91 $\pm$ 0.51 | 3.68 $\pm$ 0.15 | 0.13 $\pm$ 0.32      | 2.34 $\pm$ 0.22      | 0.42 $\pm$ 0.08      | 1.26 $\pm$ 0.17    | 1.07 $\pm$ 1.05      | 0.58 $\pm$ 0.12    | 1.59 $\pm$ 3.83      | 0.52 $\pm$ 1.00      | 11.41 $\pm$ 1.96   |
| 6517               | 2.62 $\pm$ 0.23 | 3.39 $\pm$ 0.38 | 1.79 $\pm$ 0.18   | —                        | 0.97 $\pm$ 0.16 | 0.85 $\pm$ 0.51 | 2.42 $\pm$ 0.15 | 0.92 $\pm$ 0.32      | 3.22 $\pm$ 0.22      | 1.36 $\pm$ 0.08      | 0.69 $\pm$ 0.18    | —                    | 0.59 $\pm$ 0.13    | —                    | —                    | 2.12 $\pm$ 1.87    |
| 6528               | 3.04 $\pm$ 0.28 | 3.04 $\pm$ 0.36 | 0.58 $\pm$ 0.18   | 8.07 $\pm$ 0.05          | 1.71 $\pm$ 0.17 | 1.72 $\pm$ 0.50 | 4.39 $\pm$ 0.15 | 1.36 $\pm$ 0.30      | 5.14 $\pm$ 0.23      | 2.67 $\pm$ 0.08      | 2.89 $\pm$ 0.21    | 1.93 $\pm$ 1.03      | —                  | —                    | 2.32 $\pm$ 0.87      | 14.78 $\pm$ 1.76   |
| 6541               | 1.96 $\pm$ 0.23 | —               | 2.09 $\pm$ 0.17   | 0.94 $\pm$ 0.04          | 0.99 $\pm$ 0.16 | 0.89 $\pm$ 0.50 | 1.46 $\pm$ 0.16 | 0.80 $\pm$ 0.31      | 4.07 $\pm$ 0.24      | 1.74 $\pm$ 0.09      | —                  | —                    | —                  | 0.64 $\pm$ 3.62      | —                    | 9.85 $\pm$ 1.86    |
| 6553               | 9.95 $\pm$ 0.33 | 1.94 $\pm$ 0.45 | 1.71 $\pm$ 0.19   | 8.27 $\pm$ 0.06          | 2.71 $\pm$ 0.17 | 1.73 $\pm$ 0.50 | 3.50 $\pm$ 0.16 | —                    | 5.93 $\pm$ 0.22      | 2.88 $\pm$ 0.08      | 1.72 $\pm$ 0.18    | 1.70 $\pm$ 1.04      | 4.85 $\pm$ 0.13    | —                    | 2.09 $\pm$ 0.90      | 16.99 $\pm$ 1.79   |
| 6864               | 1.26 $\pm$ 0.24 | 0.73 $\pm$ 0.37 | 2.49 $\pm$ 0.17   | 2.56 $\pm$ 0.04          | 0.87 $\pm$ 0.16 | 0.50 $\pm$ 0.51 | 0.78 $\pm$ 0.16 | 0.72 $\pm$ 0.30      | 5.00 $\pm$ 0.22      | 1.71 $\pm$ 0.08      | —                  | 0.78 $\pm$ 1.06      | 0.64 $\pm$ 0.19    | —                    | 2.64 $\pm$ 0.90      | 3.76 $\pm$ 1.95    |
| 7078               | —               | 0.21 $\pm$ 0.37 | 1.94 $\pm$ 0.18   | 0.57 $\pm$ 0.04          | 0.10 $\pm$ 0.17 | 0.10 $\pm$ 0.51 | 1.49 $\pm$ 0.16 | —                    | 1.60 $\pm$ 0.22      | —                    | —                  | —                    | 6.24 $\pm$ 0.13    | —                    | —                    | 2.31 $\pm$ 1.93    |

**Figure 6.** Examples of line limits and continuum band-passes. The labels (a), (b), (c), (d), (e) and (f) indicate the cluster from which they were taken, being: NGC 104, NGC 6388, NGC 6528, NGC 6440, NGC 7078 and NGC 6553, respectively.

### 3.3 Observations compared to models

Theoretical spectral models for SSPs have become fundamental in studies of the stellar population of galaxies. Thus, as more such models are available, it becomes increasingly important to test them over all the spectral wavelengths (Cid Fernandes & González-Delgado 2010). Our main goal in this paper is to compare the integrated spectra of actual globular clusters with theoretical predictions of M05 models. These models were chosen due to the fact that up to date they are the only ones that make predictions about the presence of almost all observed absorption lines and bands in the NIR spectral region.

In order to compare observations with models we measured in M05 models the same set of  $W_\lambda$  (using our continuum and line definitions) as in the star clusters. The  $W_\lambda$  of the optical absorption features were also measured on the models using the definitions described in Sec. 3.2.

Indices, such as  $W_\lambda$  of spectral absorption lines, can be seen as a compressed, but highly informative, representation of the whole spectrum (Cid Fernandes 2007). Thus, they are one of the more suitable ways to compare the observables with model predictions. To compare observations with models, NIR spectral indices (this work), were plotted against each other and versus optical  $W_\lambda$ . Some of the most significant correlations are shown in Fig. 7, together with model predictions.

In Fig. 7a we compare the relation between NIR Fe I 1.58  $\mu$ m and the optical Fe I 4531 Å with model predictions. The shaded region represents the model values for ages from 4 up to 15 Gyr (dotted and solid lines represent the limits), with metallicities between  $\frac{1}{200} Z_\odot$  and  $2 Z_\odot$ . Clearly, the models can reproduce the  $W_\lambda$  of the optical Fe I absorption line of the star clusters (i.e. old ages and  $Z \leq Z_\odot$ ). However, they only predict the values of the NIR Fe I line in about half of our sample. Similar conclusions are obtained when considering Figs. 7b and 7c, in the latter case, however, for the NIR Si I line.

Cid Fernandes & González-Delgado (2010) have shown the importance of modelling the horizontal branch to properly estimate the origin of blue stellar populations in integrated light analyses. As M05 models consider the blue horizontal branch, we include such models in Fig. 7a (open triangles joined by a dashed line). Note that we have only included the 15 Gyr old population because the 4 Gyr models are not available for all metallicities. No significant differences are observed in the prediction of blue horizontal branch and standard models in the case of the Fe I and Si I lines (Figs. 7a to 7c).

Similarly to Fig. 7a, we compare the optical G band and the 2.29  $\mu$ m CO band in Fig. 7d. As in the case of the Fe I lines, the observed optical band values are almost all in agreement with the model predictions. However, in the case of the 2.29  $\mu$ m CO band, the models predict lower values than the observations for  $\sim 50\%$  of the sample. A similar trend occurs for H $\beta$  (Fig. 7e) and Na I 5895 Å (Fig. 7f).

Regarding the presence of blue horizontal branch stars in the models, they do describe better the optical absorption, i.e. they predict lower values for the G band. As expected, they also play an important role in determining the  $W_\lambda$  of H $\beta$ . In contrast, the blue horizontal branch models follow the standard ones concerning the Na I line (Fig. 7f).

The NIR Mg I line and the optical Mg<sub>2</sub> are compared with the models in Fig. 7g. As for the Iron lines, the optical feature is properly predicted by the models, while they fail in the case of the NIR Mg I line, since in this case the predicted values are about one or

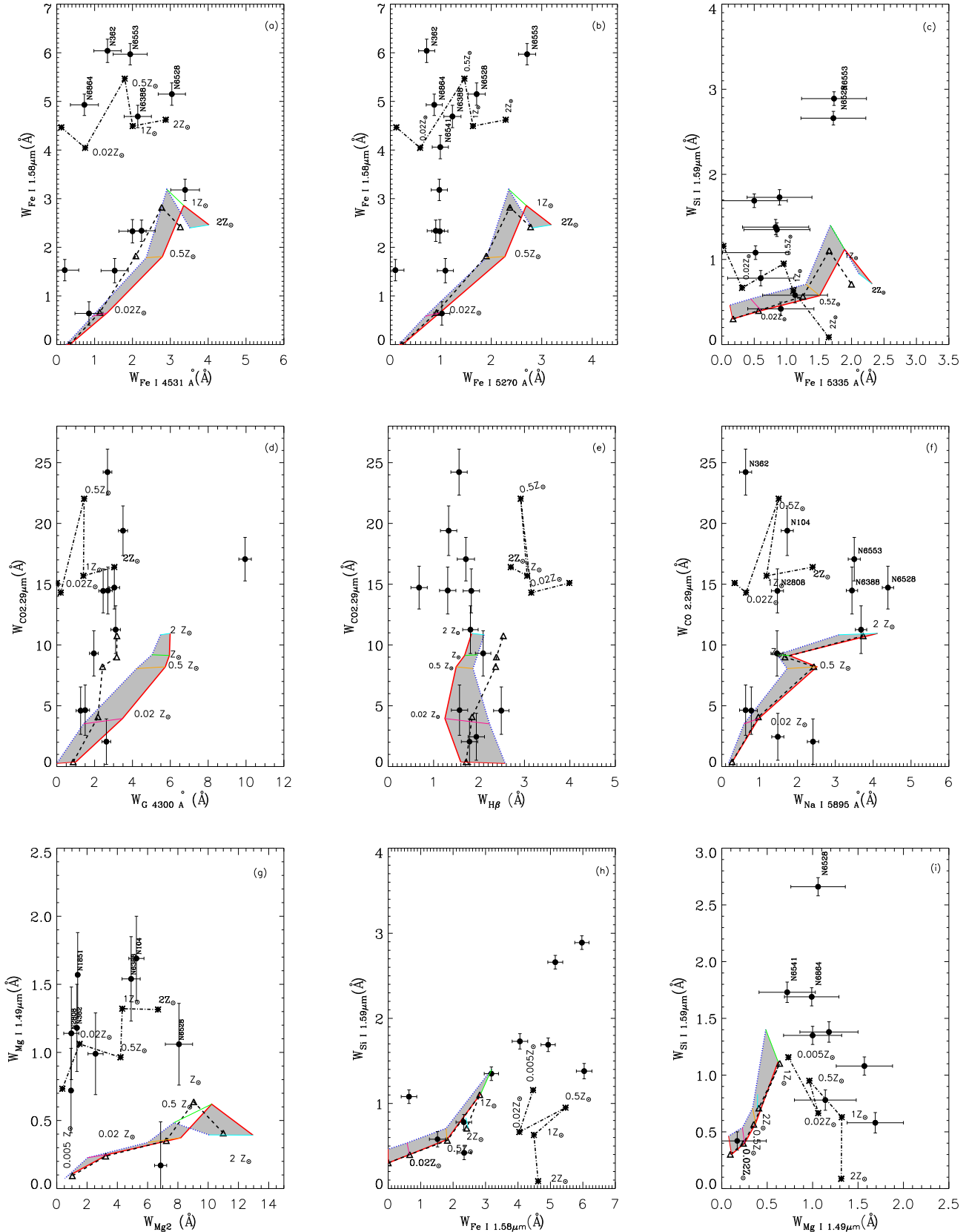


**Figure 7.** Comparison of the measured  $W_\lambda$  with model predictions. The shaded region represents models predictions for ages from 4 up to 15 Gyr (dotted and solid lines represent the limits), with metallicities between  $\frac{1}{200} Z_\odot$  and  $2 Z_\odot$ . Open triangles joined by a dashed line represent models which consider the blue horizontal branch. Asterisks joined by the dot-dashed line represent models with 1 Gyr old. Metallicities are labelled, except the lowest value, which we left out for display purposes.

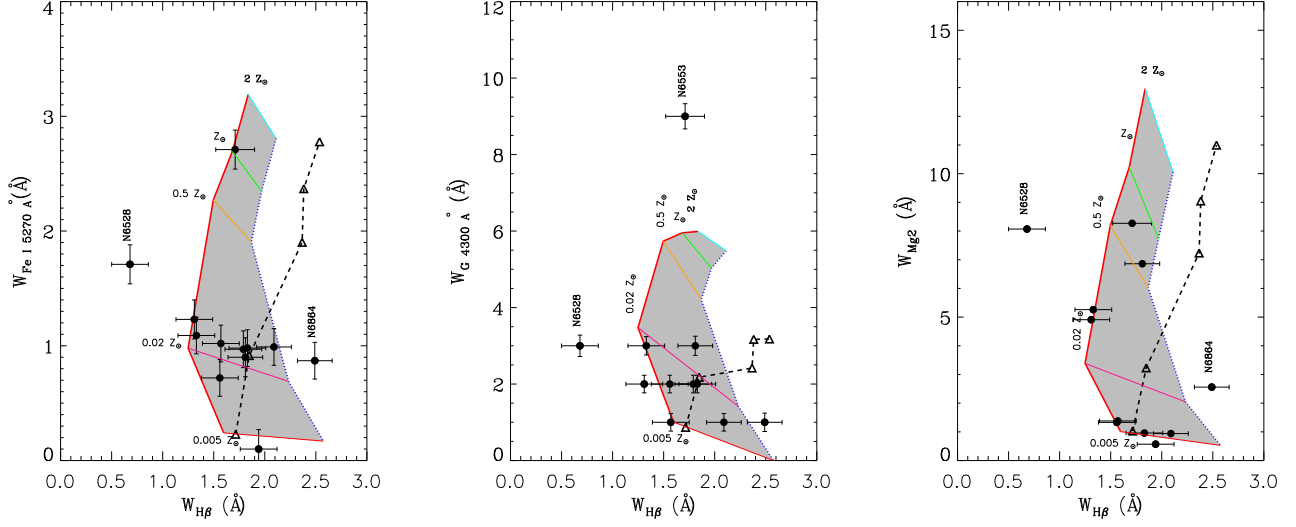


**Figure 8.** Same as Fig. 7 but for optical  $W_\lambda$  and without the 1 Gyr models.

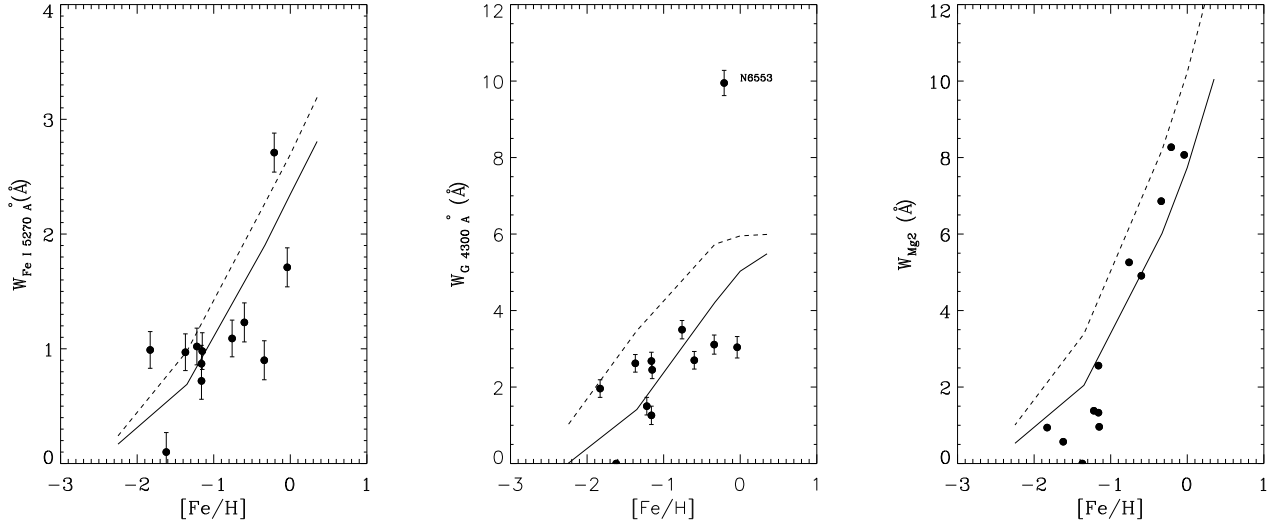


**Figure 9.** Dependence of selected optical indices on  $[\text{Fe}/\text{H}]$ . Full and dashed lines are 4 Gyr and 13 Gyr old models, respectively.

der of magnitude lower than the observations. The blue horizontal branch models follow the standard ones.

In Fig. 7h and 7i we compare NIR absorption lines against each other. It is clear that the models do not reproduce the observed strengths for Mg I  $1.49\mu\text{m}$ . However, as discussed above they do describe the measured values for Fe I  $1.58\mu\text{m}$  and Si I  $1.59\mu\text{m}$  in about half of the sample. As expected, the blue horizontal branch models are very similar to the standard ones.

We also check the M05 models in the optical by comparing the  $W_\lambda$  of optical absorption lines against each other in Fig. 8. Clearly, the models reproduce the absorption line strengths measured in almost all objects. Although a dependence on metallicity is already apparent in Figs. 8-7, we show this more explicitly Fig. 9, for selected optical indices. Both Fe I  $5270\text{\AA}$  and  $\text{Mg}_2$  present a mild correlation with  $[\text{Fe}/\text{H}]$  that, to a lesser degree, also applies to the G-band. The M05 models are sensitive to metallicity, and they do re-

produce the observations. It is worth mentioning that there are two outliers in Fig. 8, NGC 6528 and NGC 6864. The former is located close to the Galactic centre and, thus,  $W_{\text{H}\beta}$  may be attenuated by reddening. Regarding NGC 6864, there is a significant contribution of blue horizontal branch stars (see Fig. 5 of Kravtsov et al. 2007), which may be enhancing the  $\text{H}\beta$  absorption.

The perception gained when considering absorption features is that M05 models, which up to date are the most suitable to describe almost all absorption lines/bands observed in the NIR, do properly reproduce the optical absorption line strengths. Regarding the NIR absorption lines, the models do underestimate the strengths of Mg I  $1.49\mu\text{m}$ , but they can properly reproduce the observed  $W_\lambda$  of Fe I  $1.58\mu\text{m}$ , Si I  $1.59\mu\text{m}$ , and CO  $2.29\mu\text{m}$ , in about half of our sample.

In the case of CO  $2.29\mu\text{m}$   $W_\lambda$ , similar results were obtained by Lyubenova (2010, see their Fig. 9) for old and metal-poor Large Magellanic Cloud (LMC) globular clusters. These authors also



show that a large fraction of carbon stars would mimic the spectrum of a younger cluster. To check this hypothesis, we overplot in Fig. 7 1 Gyr models (asterisks joined by dot-dashed line). Interestingly, the intermediate age models can describe the observed  $W_{\text{CO } 2.29\mu\text{m}}$  in about half of our sample. Thus, we suggest that the NIR light in the core of these clusters (NGC 104, NGC 362, NGC 2808, NGC 6388, NGC 6528, NGC 6553) may, perhaps, be dominated by C-rich stars. Note that, the metallicity distribution of the clusters is heterogeneous (see Tab. 2), thus these large values of  $W_{\lambda}$  of the CO 2.29 $\mu\text{m}$  are probably not related to metallicity. This suggests a possible carbon-fraction/age degeneracy that affects NIR stellar populations. Indeed, according to Marigo et al. (2009) (see their Fig. 5), the  $K$  luminosity fraction of TP-AGB stars in 10 Gyr old SSPs of different metallicities has been shown to grow from about 15% (at  $[Z/Z_{\odot}]=0.0$ ) to 50% (at  $[Z/Z_{\odot}]=-2.3$ ). We remind that the 1 Gyr models in Fig. 7 are not related to cluster age. Instead, they simply reflect the presence of C-rich stars in some globular clusters. Also, it is interesting to remark that C-rich stars are only important in the NIR, being essentially unnoticed in the optical (see Fig. 8).

Interestingly, the Fe I 1.58  $\mu\text{m}$  atomic lines are well reproduced by the 1 Gyr population in about half of the sample (NGC 362, NGC 6388, NGC 6528, NGC 6553 and NGC 6864). In the case of Mg I 1.49 $\mu\text{m}$ , it occurs for almost all objects (NGC 104, NGC 2808, NGC 6388, NGC 6528 and NGC 6864). This suggests that the inclusion of empirical spectra of C- and O-rich stars in the models may also have an important effect in the strength of metallic lines. Another possibility lies in the fact that we are studying  $\alpha$ -enhanced Galactic globular clusters and, as the models do not include  $\alpha$ -enhancement, this might explain why the models cannot reproduce the  $W_{\lambda}$  of absorptions involving  $\alpha$ -elements.

Another powerful way to test SSPs models is by comparing observed and predicted colours. For this purpose, we collected the optical to NIR colours of our star clusters from the literature. These values are listed in Tab. 2, together with some basic properties of the cluster sample.

We compare the observed colours with the models prediction in Fig. 10. Note that the optical colours were reddening-corrected using the Cardelli, Clayton & Mathis (1989) extinction law, and the  $E(B-V)$  values from Bica et al. (2006). Clearly if standard errors, in colours, are taken into account, the models are able to describe almost all the observations. However, there are some outliers (NGC 6440, NGC 6517, NGC 6528 and NGC 6553) for which it is not possible to determine whether or not the models apply, or if the photometric uncertainties are large, since these objects are located very close to the Galactic centre, and thus are more likely contaminated by field stars. Note that these objects are located in the Galaxy bulge (see Tab. 2), and therefore, precise measurements are difficult. In addition, uncertainties in SSPs due to stellar tracks and EPS codes in the  $V - K$  colour are typically 0.25 mag (see Charlot et al. 1996, M05). In this way, we suggest that M05 models, in general, are able to predict the observed color values for the optical. For the NIR, however, they do systematically predict bluer colours, and a 2 Gyr SSP is required to properly reproduce the observed NIR colours. Thus, they may underestimate the age for the old population.

The above results lead us to conclude that M05 models can provide reliable information on the NIR stellar population of galaxies only when  $W_{\lambda}$  and colours are taken together, in other words,  $W_{\lambda}$  and continuum fluxes should be simultaneously fitted (e.g. Riffel et al. 2008), alternatively the whole underlying spectrum should be used (e.g. Riffel et al. 2009, 2010; Martins et al. 2010).

However, the results should be taken with caution, since the models tend to predict results biased towards young ages. A more robust test is fit the whole globular clusters spectra with models. However, this is out of the scope of this paper and we leave it for a forthcoming publication (Ruschel-Dutra et al., 2010 *in preparation*).

## 4 CONCLUSIONS

We use NIR SOAR/OSIRIS integrated spectra of 12 Galactic globular clusters to test M05 NIR EPS models, and to provide spectral observational constraints to calibrate future NIR EPS models. M05 models are used for being, up to date, the most suitable to describe absorption lines/bands in the NIR. Our main conclusions are:

- The spectra of the cluster sample appear qualitatively similar in most of the NIR absorption features.
- Many atomic absorption features like:  $\lambda$  1.49 $\mu\text{m}$  Mg I,  $\lambda$  1.58 $\mu\text{m}$  Fe I/Mg I,  $\lambda$  1.59 $\mu\text{m}$  Si I,  $\lambda$  1.71 $\mu\text{m}$  Mg I,  $\lambda$  2.21 $\mu\text{m}$  Na I and  $\lambda$  2.26 $\mu\text{m}$  Ca I as well as the  $\lambda$  1.62 $\mu\text{m}$ ,  $\lambda$  2.29 $\mu\text{m}$  CO and  $\lambda$  2.05 $\mu\text{m}$  CN molecular bands are clearly detected and identified in the spectra. The  $W_{\lambda}$  of these features were measured, as well as the optical  $W_{\lambda}$  of G band (4300 $\text{\AA}$ ), MgH (5102 $\text{\AA}$ ), and FeI (4531 $\text{\AA}$ ). The globular clusters observations ( $W_{\lambda}$  and colours) were compared with models predictions with ages from 4 up to 15 Gyr, with metallicities between  $\frac{1}{200} Z_{\odot}$  and  $2 Z_{\odot}$ .
- M05 models are able to properly reproduce the optical  $W_{\lambda}$  observed in globular clusters.
- The models do underestimate the strength of Mg I 1.49 $\mu\text{m}$ , but they can properly reproduce the observed  $W_{\lambda}$  of Fe I 1.58 $\mu\text{m}$ , Si I 1.59 $\mu\text{m}$  and CO 2.9 $\mu\text{m}$  in about half of our sample. For the remaining objects, we needed to consider intermediate-age populations. Thus, we suggest that the presence of C- and O-rich stars in the models is important to reproduce the observed strengths of metallic lines. Another possibility is the lack of  $\alpha$ -elements enhancement in the models.
- No significant differences are observed in the prediction of blue horizontal branch and standard models in the case of the Fe I lines (optical and NIR). A similar trend is observed for the Na I 5895 $\text{\AA}$ . While in the case of the G-band the models which include blue horizontal branch do describe better the observations. No differences between blue horizontal branch and standard models are found for the NIR observations.
- In general, M05 models can reproduce the observed colours in the optical, while in the NIR they tend to underestimate the age of the old population.

The NIR spectral region is the most convenient one to study the stellar content of highly obscured sources. Thus, well calibrated and accurate NIR models is fundamental. Besides, observations using adaptive optics, to properly correct for atmosphere effects, have become commonly used in the NIR region, thereby allowing for high quality spectroscopy (e.g. Riffel et al. 2010). The availability of detailed, high spectral resolution, and well calibrated stellar population models in the NIR will open a new window to disentangle the NIR stellar content in the inner few pc of nearby galaxies. Thus, the data presented in this paper will be important for the new generation of NIR EPS models.

## ACKNOWLEDGEMENTS

We thank an anonymous referee for interesting comments. R.R. thanks for the support from the Brazilian funding agency Capes

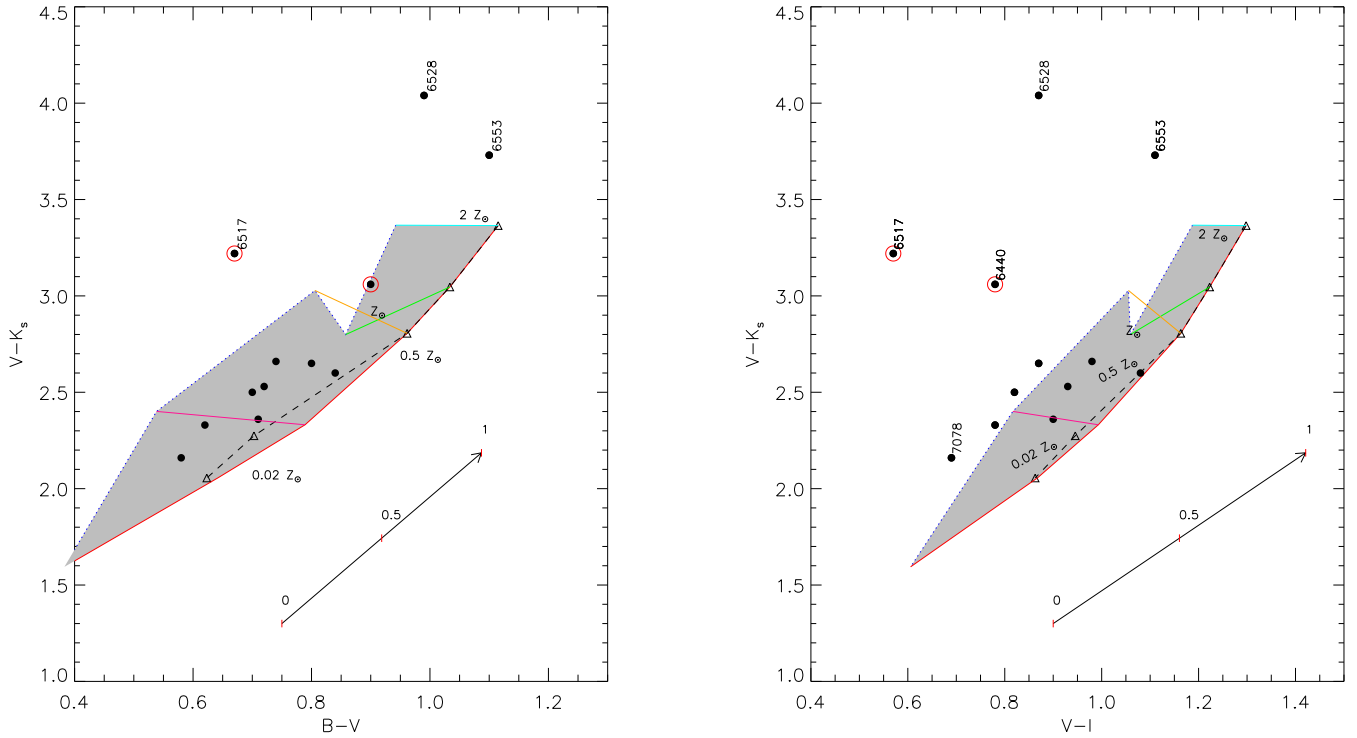


**Figure 10.** Colour-Colour diagrams. Open circles indicate objects with  $E(B-V) > 1.0$ . A reddening vector is shown for  $0 \leq A_V \leq 1$ . The lines are the same as in Fig 7, but the young age is 2 Gyr.

and CNPq. The authors are grateful to C. Maraston for useful discussions. JFCSJ thanks Brazilian agency FAPEMIG (grant APQ00117/08). ARA thanks to CNPq for partial support through grant 308877/2009-8. This work has been done with observations from the SOAR telescope, a collaboration among The Ministério da Ciência e Tecnologia/Brazil, NOAO, UNC and MSU.

## REFERENCES

- Asari, N. V., Cid Fernandes, R., Stasińska, G., Torres-Papaqui, J. P., Mateus, A., Sodr , L., Schoenell, W., Gomes, J. M., 2007, MNRAS, 381, 263
- Bica, E.; Bonatto, C.; Barbuy, B.; Ortolani, S. 2006, A&A, 450, 105
- Bica, E.; Alloin, D., 1986, A&A, 162, 21.
- 1988, A&A, 195, 76
- Bonatto, C., Bica, E., Girardi, L. 2004, AA 415, 571
- Bruzual, G. & Charlot, S., 2003, MNRAS, 344, 1000.
- Charlot, S.; Worthey G.; Bressan A., 1996, ApJ, 457, 625
- Cardelli, J. A., Clayton, G. C., Mathis, J. S., 1989, ApJ, 345, 245
- Cid Fernandes, R., Gu, Q., Melnick, J., Terlevich, E., Terlevich, R., Kunth, D., Rodrigues Lacerda, R., J     , B., 2004, MNRAS, 355, 273
- Cid Fernandes, R., Mateus, A., Sodr , Laerte, Stasińska, G., Gomes, J. M., 2005a, MNRAS, 358, 363 (CF05)
- Cid Fernandes, R., Gonz     Delgado, R. M., Storchi-Bergmann, T., Martins, L. Pires & Schmitt, H., 2005b, MNRAS, 356, 270.
- Cid Fernandes, R., 2007, arXiv:astro-ph/0701902
- Cid Fernandes, R., Schoenell, W., Gomes, J. M., Asari, N. V., Schlickmann, M., Mateus, A., Stasińska, G., Sodr , L., Torres-Papaqui, J. P., for the SEAGal collaboration, 2008, arXiv:0802.0849
- Cid Fernandes, R.; Gonz     Delgado, R. M., 2010, MNRAS, 403, 780.
- Cesetti, M.; Ivanov, V. D.; Morelli, L.; Pizzella, A.; Buson, L.; Corsini, E. M.; Dalla Bont , E.; Stiavelli, M.; Bertola, F., 2009, A&A, 497, 41.
- Cohen, Judith G.; Hsieh, Scott; Metchev, Stanimir; Djorgovski, S. G.; Malkan, M., 2007, AJ, 133, 99.
- Faber, S. M., Friel, E. D., Burstein, D., & Gaskell, C. M. 1985, ApJS, 57, 711
- Frogel, J. A.; Stephens, A.; Ramirez, S. & DePoy, D. L., 2001, AJ, 122, 1896.
- Harris, W.E. 1996, AJ, 112, 1487
- Kravtsov, V.; Alca  no, G.; Marconi, G.; Alvarado, F., 2007, A&A, 469, 529.
- Lyubenova, M.; Kuntschner, H.; Rejkuba, M.; Silva, D. R.; Kissler-Patig, M.; Tacconi-Garman, L. E.; Larsen, S. S., 2010, A&A, 510, 19
- Maraston, C., 1998, MNRAS, 300, 872.
- Maraston, C. 2005, MNRAS, 362, 799 (M05).
- Marigo P., Girardi L., Bressan A. et al. 2009, in Stellar Populations - Planning for the Next Decade, IAU Symp. 262, G. Bruzual & S. Charlot ed., p. 36
- Martins, L.; Riffel, R.; Rodr          , A.; Gruenwald, R.; de Souza, R., 2010, arXiv:1005.3562
- Moorwood, A.; Moneti, A. & Gredel, R., 1991, Msngr, 63, 77.
- Iben & Renzini 1983, ARA&A, 21, 271.
- Origlia, L.; Ferraro, F. R.; Fusi Pecci, F.; Oliva, E., 1997, A&A, 321, 859.
- Origlia, L.; Moorwood, A. F. M. & Oliva, E., 1994, Msngr, 75, 21

- Origlia, L.; Moorwood, A. F. M. & Oliva, E., 1993, *A&A*, 280, 536.
- Oliva, E., Origlia, L., Kotilainen, J. K., Moorwood, A. F. M., 1995, *A&A*, 301, 55.
- Oliva, E.; Origlia, L., 1992, *A&A*, 254, 466.
- Origlia, L.; Rich, R. M. & Castro, S., 2002, *AJ*, 123, 1559.
- Origlia, L.; Valenti, E.; Rich, R. M.; Ferraro, F. R., 2006, *ApJ*, 646, 499.
- Origlia, L. & Oliva, E., 2000, *NewAR*, 44, 257
- Riffel, R., Pastoriza, M. G., Rodríguez-Ardila, A. & C. Maraston, 2007, *ApJ*, 659L, 103
- Riffel, R., Pastoriza, M. G., Rodríguez-Ardila, A. & C. Maraston, 2008, *MNRAS*, 388, 803.
- Riffel, R., Pastoriza, M. G., Rodríguez-Ardila, A. & C. Bonatto, 2009, *MNRAS*, 400, 273.
- Riffel, R., A.; Storch-Bergmann, T.; Riffel, R.; Pastoriza, M. G., 2010, *ApJ*, 713, 469.
- Schmidt, A. A., Copetti, M. V. F., Alloin, D. & Jablonka, P., 1991, *MNRAS*, 249, 766.
- Stephens, A. W. & Frogel, J. A., 2004, *AJ*, 127, 925
- Santos, J., F. C., Jr.; Alloin, D.; Bica, E.; Bonatto, C. J., 2002, *IAUS*, 207, 727.
- Vale, T. B., Riffel, R., Pastoriza, M. G., Santiago, B. X., 2007, *Boletim da Sociedade Astronômica Brasileira*, 27, 205.
- Vollmann, K. & Eversberg, T., 2006, *AN*, 327, 862.
- Vazdekis, A.; Sánchez-Blázquez, P.; Falcón-Barroso, J.; Cenarro, A. J.; Beasley, M. A.; Cardiel, N.; Gorgas, J.; Peletier, R. F., 2010, *MNRAS*, 404, 1639
- Worthey, Guy; Faber, S. M.; Gonzalez, J. Jesus; Burstein, D., 1994, *ApJS*, 94, 687.